EXPERIMENTAL-NUMERICAL EVALUATION OF TENSILE-SHEAR RESPONSE IN RESISTANCE SPOT WELDING OF AISI 304L STAINLESS STEEL JOINTS

O. S. Barrak[1,2], S. Chatti[1*], S. Ben-Elechi[1]

[1]Laboratory of Mechanical Engineering, National Engineering School of Monastir, Monastir, Tunisia
[2]Polytechnic College of Engineering - Baghdad, Middle Technical University, Baghdad, Iraq
*Corresponding author's e-mail address: sami.chatti@udo.edu

ABSTRACT

This study investigated the influence of resistance spot welding (RSW) on the tensile-shear strength of stainless steel AISI 304L joints and was carried out using experimental and FE analyses. The mechanical properties were determined by a tensile shear test of RSW on AISI 304L sheet under different conditions (welding current, weld time, squeeze time, and hold time). The results showed that heat input, mainly controlled by welding current and welding time, was the main factor influencing nugget formation and the load-bearing capacity. A 3D FE model with a close-to-reality mesh of the nugget-HAZ interface was prepared to match the test conditions. The model demonstrated a ring-shaped stress zone along the edge of the nugget and was consistent with the pull-out failure observed in the experiment. The experimental results with errors (3.5–4.8%) and observations can be used to ensure that a properly calibrated FE model can predict RSW performance in AISI 304L and possibly aid in weld parameter optimization. The results provide an effective means of evaluating welds through experiments and simulations.

KEYWORDS: finite element, resistance spot welding, tensile-shear, AISI 304L

1. INTRODUCTION

Resistance Spot Welding (RSW) is a widely used joining technique for sheet assemblies in various industries such as automotive, aerospace, household appliances, and lightweight structures. RSW is highly productive, easy to automate, and has low operating costs. Stainless steel AISI 304L is the most used material for RSW due to its stability, corrosion resistance, and work-hardenability. These qualities make stainless steels a good choice for applications that require energy efficiency and fatigue resistance [1-4]. The mechanical properties of RSW joints in AISI 304L sheets depend on factors such as weld current, welding time, squeeze time, and hold time. These settings affect the heat input during welding, which in turn influences nugget growth, fusion quality, local mechanical properties, the microstructure in the nugget and heat-affected zone (HAZ), and, respectively, the loads, the tensile-shear strength of the joint, and the long-term reliability of the assembly [5-6].

Testing only the tensile-shear behaviour does not fully explain how stress is redistributed inside the nugget and along the fusion boundary. Because of this, finite-element-based simulation (FEM / FEA) is now used alongside experiments to better understand strain localization, stress paths, and how failure starts in RSW stainless steels. For AISI 304 series RSW joints, combining experimental and numerical methods is recommended to reduce the cost of destructive testing, accelerate parameter screening, and predict weld quality [7-10]. Although RSW is widely used in industrial AISI 304L structures, there has been little research combining experimental and finite-element analyses of the tensile-shear response of RSW in AISI 304L, using a controlled DOE with real production welding parameters. In particular, the direct quantitative link between shear stress, weld nugget shape, and FE-predicted stress fields has not been fully studied. As a result, further investigation is still needed [11-13]. Besides tensile-shear response, the nugget zone in austenitic stainless steels shows complex solidification due to δ-ferrite formation, Cr-Mo partitioning, and dendritic sub-grain refinement. These factors can significantly affect interfacial strength and fracture behaviour [14-15]. The 304L grade conducts heat and electricity well, so its higher thermal conductivity compared to ferritic or low-carbon steels leads to a non-uniform thermal field during spot welding. The shape and structure of the nugget are highly dependent on process settings. Therefore, the use of FEM for quantitative prediction is essential not only to locate the stress concentration but also to correlate thermal history, microstructural evolution, and ultimate weld strength. Such modelling is widely used in digital welding process control and quality prediction systems [16-17].

Date of submission/acceptance: 09.11.2025/15.12.2025
https://doi.org/10.35219/awet.2025.10

The simulation for modern industry, such as digital validation, virtual qualification, and physics-based optimization of manufacturing processes, is showcased to verify the perspective for stainless steel spot welds; we discuss their application. This is of particular interest for the Body-in-White structures of automotive vehicles that consist of thousands of welds required to resist crash, vibration, and high-cycle fatigue loading at the same time. The approach is a mix of physical testing and numerical stress mapping, which supports the development of optimized resistance spot welding process windows for production. After being validated, the finite element predictions are applied to actual tensile-shear test results to promote a more united, reasonable weld quality prediction of stainless steel assemblies [18-20]. Many studies on RSW have been published, but most focus on either tensile-shear strength or nugget development in isolation. Several also use simplified FE models that do not fully show the stress distribution at the nugget–HAZ interface.

This study uses a controlled DOE for welding parameters along with a calibrated 3D FE model. This model shows the nugget geometry and boundary conditions, giving a more realistic connection between heat input and localized shear stress during failure. The tensile-shear response of resistance spot welding (RSW) AISI 304L joints has been studied using an experimental approach and finite element (FE) simulations.

The study developed experimental conditions and process parameters based on the industrial RSW process. The tensile-shear tests of the AISI 304L welded specimens fabricated at different welding currents, welding times, squeeze times, and hold times are carried out and simulated by employing a three-dimensional finite element (FE) model.

The model uses the same boundary conditions and load sequence as in the test, so a direct comparison can be made, and the model's accuracy can be finely assessed.

2. EXPERIMENTAL METHODS

The material employed in the study was stainless steel AISI 304L, whose composition was analyzed by a laboratory, as shown in table 1. The physical properties of the materials, evaluated according to standard test methods, are reported in table 2. Sample sizes followed the standards in AWS of resistance spot welding joints [21-22]. The prepared sheets (100 × 25 mm, thickness is 1 mm) are displayed in figure 1 [22]. The sheets were cut and mechanically ground to remove oxide layers. Before welding, the surfaces were cleaned with an ethanol-acetone solution to ensure good electrical contact and reduce surface resistance. All shear test specimens had an overlap of 25 mm, which formed a single-lap joint for the tensile-shear test. Welding was performed using a resistance spot welding machine equipped with Cu–Cr domed electrodes having tip diameters of 6 mm (coded A). Process parameters varied for different specimen sets [22]. These included combinations of welding current (kA), welding time (s), squeeze time (s), and hold time (s).

In this study, the Taguchi method was used to design the welding parameter matrix shown in figure 2. This approach was chosen because it lets test several welding parameters efficiently, using fewer but still representative specimens. For each welding condition, three specimens were produced and tested to assess repeatability and accounts for measurement differences. varied welding current, welding time, squeeze time, and hold time independently, following the Taguchi technique.

This setup helped evaluate each factor's effect without overlap, providing a reliable means to assess the mechanical response of the RSW joints. Figure 2 shows a matrix of these input variations, which observes their effects on weld nugget formation, fusion profile, and tensile-shear properties. A constant electrode force was used in all welding specimens to prevent indentation and reduce the chance of expulsion.

Table 1. Chemical composition of AISI 304L

Element wt [%]	C	Si	Ni	P	S	Cr	Mo	Mn	V	Cu	Fe
AISI 304L	0.027	0.52	11.24	0.032	0.005	18.89	0.002	1.53	0.008	0.246	Bal.

Table 2. Material properties of AISI 304L

Material Property	AISI 304L
Yield strength [MPa]	305
Tensile strength [MPa]	610
Elongation El. [%]	62
Young's modulus [GPa]	193
Density [kg/m^3]	8000
Poisson's ratio	0.28
Thermal conductivity [W/m·K]	16.2
Coefficient of thermal expansion [K]	$17.2 \cdot 10^{-6}$
Heat capacity at constant pressure [J/kg·K]	500
Electrical conductivity [S/m]	$1.4 \cdot 10^{6}$
Relative permittivity	1.005

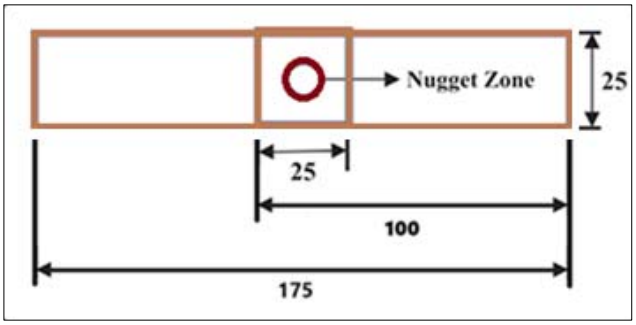

Fig. 1. Test specimen dimensions (in mm)

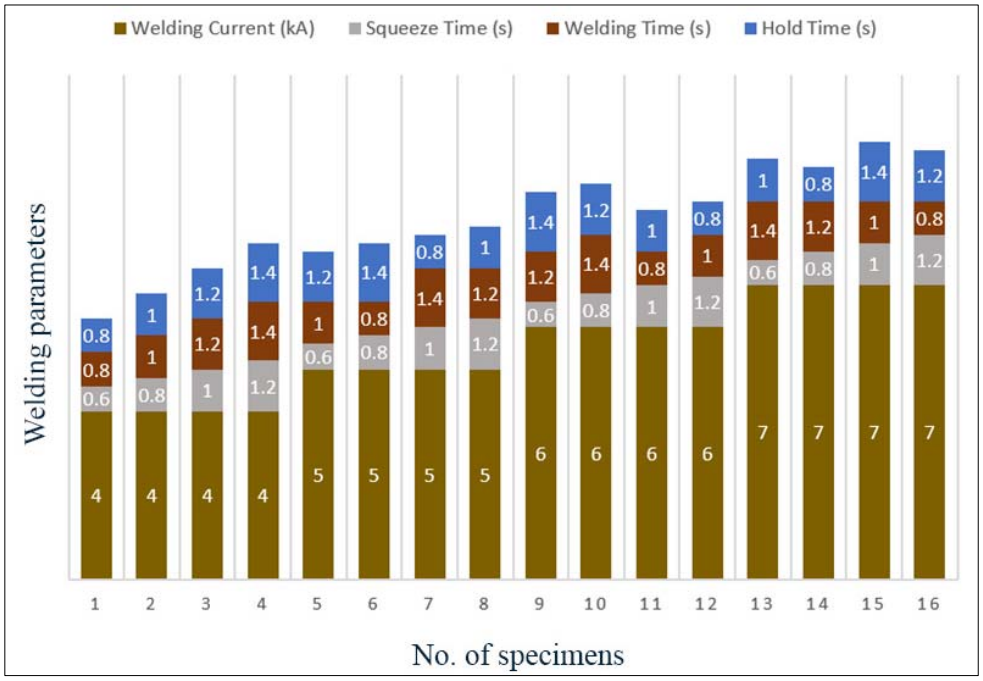

Fig. 2. Welding parameters of RSW

2.1. Tensile-Shear Tests

Tensile-shear tests were conducted on a universal testing machine (UTM) using displacement-controlled loading at 1 mm/min, in accordance with ASTM standards for welded evaluation [21]. Each specimen was placed in a tensile-shear fixture so the force was applied parallel to the sheet and directly across the weld nugget.

2.2. Tensile-Shear Simulation

A 3D finite element model was built to simulate the tensile-shear test on AISI 304L RSW joints and compare the results with experimental data. The finite element model used a full tetrahedral mesh with 12,702 elements and 4,483 vertices. The average element quality was 0.4866, with a minimum of 0.2358. Along the sheet boundaries, there were 8,788 triangle elements. The total mesh volume was 5499 mm³. This mesh density provided enough detail around the weld and lap interface, where stress tends to concentrate during tensile-shear loading. The selected mesh resolution is stable and works well for nonlinear stress analysis of RSW joints.

The mechanical properties used in the FE model were taken from table 2. The model used an isotropic elastic-plastic material with bilinear hardening to represent both the initial elastic deformation and the later plastic shear flow.

The numerical process started with a welding simulation that created the thermal field and showed how the material softened in the weld area. This initial step allowed the model to estimate changes in mechanical behavior in the nugget and HAZ, including local drops in yield strength and changes in ductility due to welding.

The results from this simulation were then used as input for the following tensile-shear simulation. This way, the finite element model shows the non-uniform mechanical properties of the welded joint rather than treating it as a uniform base material.

3. RESULTS AND DISCUSSION

3.1. Tensile Shear Test

Figure 3 displays the appearance of AISI 304L welded samples after the tensile-shear test. All joints showed the usual nugget pull-out failure, with no expulsion or major tearing. This indicates the formation of stable fusion boundaries and good metallurgical bonding with the chosen process parameters.

Figure 4 shows the tensile-shear force values for the welded samples. The samples welded with the best parameter combination had the highest strength, showing that welding current and time most affect joint strength. When the heat input increased, the nuggets became larger and more uniform. This also improved their ability to handle shear deformation along the interface, while too little heat led to a smaller nugget and weaker joints. This pattern matches reports in the literature about the key role of current-controlled heat in the strength of austenitic stainless steel RSW joints [2], [16]. The results also show that stainless steels like AISI 304L benefit from more heat at the nugget because they have higher resistivity and lower thermal conductivity than ferritic steels.

To simulate and validate the FE model, we selected three specimens from the full dataset in Figure 4: specimen no. 12, which had the highest tensile-shear force; specimen no. 3, which had the lowest; and specimen no. 8, which had a value in between. By selecting these, the model was tested across the full range of welded-joint performance, not just a single condition. This approach helps confirm that the model captures mechanical responses across low, medium, and high-strength cases while maintaining a reliable, efficient verification process.

Fig. 3. Specimens after the tensile-shear test

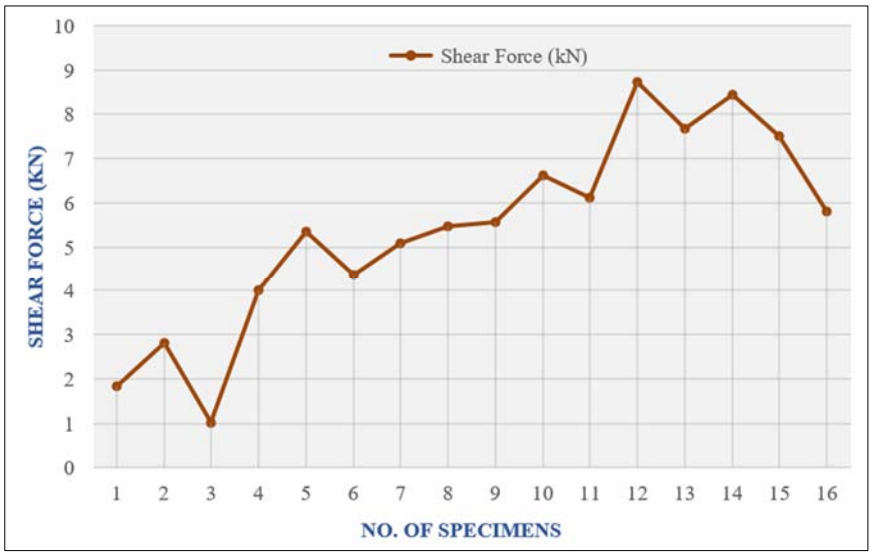

Fig. 4. Tensile-shear force

3.2. Tensile Shear Simulation

Figure 5 shows the numerical stress distribution from the 3D finite element tensile-shear model of the AISI 304L lap joint. The highest von Mises stresses appeared along the nugget–HAZ boundary, forming a ring of plastic deformation, which matches the stress localization zones reported in RSW FE modelling studies [13], [15]. The nugget core had lower equivalent stress, which confirms that fractures start with shear-band formation around the fusion boundary, not from uniform yielding in the nugget. These results show that the stress-transfer path predicted by the FE model matches that observed in experiments.

The finite element simulation enabled visualization of stress distribution in the nugget and the surrounding heat-affected zone during tensile-shear loading. When a shear load was applied to the lap joint, the model showed uneven deformation. Shear stress built up mostly around the edge of the fusion zone, not in the centre of the nugget. This zone of stress, known as the load-transfer belt, is where most of the plastic

shear flow occurs prior to the development of a macroscopic crack.

The simulation results indicate that the maximum von Mises stress is found at the boundary of the weld nugget, consistent with the experimentally observed fracture locations. This indicates that the fracture initiates at the interface between the nugget and HAZ rather than within the centre of the fusion zone. This is reasonable; the nugget possesses a more homogeneous microstructure, whereas the HAZ features variations in hardness, grain morphology, and residual thermal stresses. Therefore, based on FE results, it can be concluded that weld failure in AISI 304L is primarily governed by shear strain concentration at the nugget boundary rather than by overall nugget shearing.

The FE strain-energy density results also showed that increasing the weld current or weld time made the nugget larger and shifted the highest stress farther out, thereby reducing the stress gradient. In simple terms, bigger nuggets spread out the stress more evenly and are less likely to start shear cracks. This matches the experimental finding that higher heat input leads to stronger welds in tensile-shear tests.

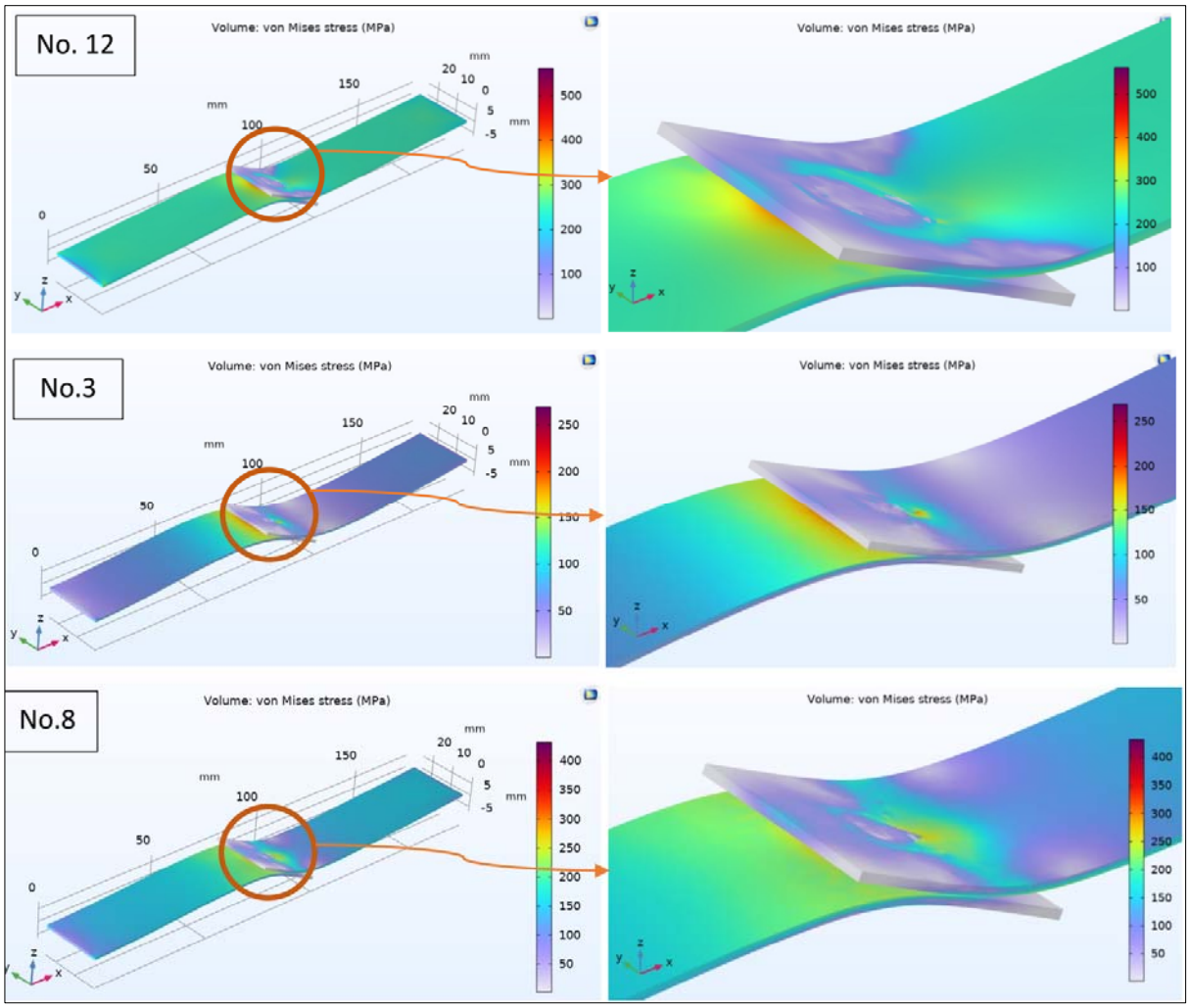

Fig. 5. Simulation of the tensile test of similar AISI 304L

3.3. Tensile Shear Validation

Table 3 shows a direct comparison between FE-predicted tensile-shear stress and experimental values for different specimen groups. The error stayed below 5% in all cases, ranging from 3.5% to 4.8%. This close match shows that the FE model accurately reflects the load-bearing behaviour of the RSW joint. Other studies on austenitic stainless steels have also reported similar low error ranges [13], [16]. Therefore, the FE model developed in this study can be used to predict the effects of weld parameters and to optimize process settings without requiring full destructive tests.

The strong agreement between experimental and numerical results also shows that combining tensile-shear lab tests and structural FE simulation is a reliable way to assess the mechanical strength of AISI 304L spot welds. This approach is important for the industry because it enables cost-effective digital validation of stainless steel assemblies with many spot welds, which are common in automotive body structures.

Table 3. Tensile-shear stress validation

No. of specimens	Simulation value [MPa]	Experimental value [MPa]	Error
12	121.01	115.46	4.8%
8	73.7	71.2	3.5%
3	52.8	50.4	4.8%

4. CONCLUSIONS

This study showed that the tensile-shear force of resistance spot welding AISI 304L joints mainly depends on heat input, which affects nugget size and the stress at the nugget-HAZ boundary. Tests confirmed that using higher welding current and longer welding time increased weld strength by forming larger, more uniform nuggets. The finite-element simulation matched the stress-concentration patterns observed in experiments, with a clear shear-strain ring at the nugget edge, consistent with the observed nugget pull-out failure mode.

The close match between the numerical and experimental tensile-shear stress values, with differences of only 3.5-4.8%, confirms that the FE model used in this study is valid. The close agreement between the numerical and experimental tensile-shear results indicates that the calibrated FE model shows the mechanical behaviour observed in the tested specimens. However, this result is limited to the welding parameters and single-sheet setup used in the tests, and should not be seen as a general prediction. The combined experimental and numerical approach in this study provides an effective way to support digital weld evaluation and can be used in industrial settings where reliable spot weld validation is needed, such as in automotive body-in-white assembly.

ACKNOWLEDGEMENTS

We would like to thank the head of the Polytechnic College of Engineering - Baghdad, Middle Technical University, Baghdad, Iraq and all the department's teaching staff for their assistance.

REFERENCES

[1] **Hamzah M. M.**, **Barrak O. S.**, **Abdullah I. T.**, **Hussein A. A.**, **Hussein S. K.,** *Process parameters influence the mechanical properties and nugget diameter of AISI 316 stainless steel during resistance spot welding*, International Journal of Applied Mechanics and Engineering, 2024, vol. 29, iss. 2, pp. 79-89.

[2] **Wang, B., Qiu F., Chen L., Zhou Q., Dong B., Yang H., Yang J., Feng Z., Tyrer N., Barber Gary C., Hu M.,** *Microstructure and shearing strength of stainless steel/low carbon steel joints produced by resistance spot welding*, Journal of Materials Research and Technology, 2022, vol. 20, pp. 2668-2679.

[3] **Barrak O. S., Ben-Elechi S.**, **Chatti S.,** *Parameters influence on mechanical properties of resistance spot welding: AISI304L/AISI1005*, Pollack Periodica, 2025, vol. 20, iss. 1, pp. 102-109.

[4] **Sar M. H.**, **Ridha M. H.**, **Husain I. M.**, **Barrak O. S.**, **Hussein S. K.,** *Influence of welding parameters of resistance spot welding on joining aluminum with copper*, International Journal of Applied Mechanics and Engineering, 2022, vol. 27, iss. 2, pp. 217-225.

[5] **Adkine A. S.**, **Biradar S. K.,** *A review of the effects of resistance spot welding on metallurgical and mechanical characteristics*, Welding International, 2025, vol. 39, iss. 2, pp. 52-65.

[6] **Elitas M.** *Effects of welding parameters on tensile properties and fracture modes of resistance spot welded DP1200 steel*, Materials Testing, 2021, vol. 63, iss. 2, pp. 124-130.

[7] **Kim S., Hwang I., Kim D.-Y., Kim Y.-M., Kang M., Yu J.,** *Weld-quality prediction algorithm based on multiple models using process signals in resistance spot welding*, Metals 2021, vol. 11, iss. 9, pp. 1459.

[8] **Barrak O. S.**, **Chatti S.**, **Ben-Elechi S.,** *Influence of Welding Parameters on Mechanical Properties and Microstructure of Similar Low-Carbon Steel AISI 1005 Welding by Resistance Spot Welding*, Journal of Technology, 2024, vol. 6, iss. 1, pp. 45-51.

[9] **Mishra D.** et al. *Dissimilar resistance spot welding of mild steel and stainless steel metal sheets for optimum weld nugget size*, Materials Today: Proceedings, 2021, vol. 46, pp. 919-924.

[10] **Sadeghian B.**, **Taherizadeh A.**, **Salehi T.**, **Sadeghi B.**, **Cavaliere P.,** *Simulation and microstructure prediction of resistance spot welding of stainless steel to carbon steel*, Metals 2022, vol. 12, iss. 11, pp. 1898.

[11] **Rached S.**, **Chaabene A.**, **Chatti S.,** *Enhancing friction stir welding performance: Finite element simulation study using filler material*, Annals of „Dunarea de Jos" University of Galati, Fascicle XII, Welding Equipment and Technology, 2024, vol. 35, pp. 79-92.

[12] **Husain I. M., Taresh O. F., Mohammed G. R. A., Barrak O. S., Hussain S. K., Kareem A. K.,** *Effect of pulses on spot resistance welding of AA1050 aluminum alloy*, AIP Conference Proceedings, 2024, vol. 3105, iss. 1, pp. 020033.

[13] **Moshayedi H.**, **Sattari-Far I.,** *Numerical and experimental study of nugget size growth in resistance spot welding of austenitic stainless steels*, Journal of Materials Processing Technology, 2012, vol. 212, iss. 2, pp. 347-354.

[14] **Pańcikiewicz K.**, **Świerczyńska A.**, **Hućko P.**, **Tumidajewicz M.,** *Laser dissimilar welding of AISI 430F and AISI 304 stainless steels*, Materials, 2020, vol. 13, iss. 20, pp. 4540.

[15] **Kumar R.**, **Chohan J. S.**, **Goyal R.**, **Chauhan P.,** *Impact of process parameters of resistance spot welding on mechanical properties and micro hardness of stainless steel 304 weldments*, International Journal of Structural Integrity, 2021, vol. 12, iss. 3, pp. 366-377.

[16] **Shawon M. R. A.**, **Gulshan F.**, **Kurny A. S. W.,** *Effect of welding current on the structure and properties of resistance spot welded dissimilar (austenitic stainless steel and low carbon steel) metal joints*, Journal of The Institution of Engineers (India): Series D, 2015, vol. 96, pp. 29-36.

[17] **Fouzi M. S. M.**, **Jelani K. M.**, **Nazri N. A.**, **Sani M. S. M.**, *Finite element modelling and updating of welded thin-walled beam*, Int. J. Automotive and Mechanical Engineering 2018, vol. 15, iss. 4, pp. 5874-5889.

[18] **Chaabene A.**, **Ben Khalifa A.**, **Chatti S.,** *Numerical simulation of microcellular injection molding: A case study*, Annals of Dunarea de Jos University of Galati, Fascicle XII, Welding Equipment and Technology 2024, vol. 35, pp. 5-24.

[19] **Saad M. L.**, **Sar M. H.**, **Barrak O. S.**, **Hussein S. K.**, **Hussein A. K.,** *Fuzzy logic model analysis of shear force in aluminium/polyethylene lap joined by hot press*, IOP Conference Series: Materials Science and Engineering 2019, vol. 518, iss. 3, pp. 032007.

[20] **Demiral M.**, **Duran E. T.,** *Failure analysis of resistance spot-welded structure using XFEM: lifetime assessment*, Applied Sciences 2023, vol. 13, iss. 19, pp. 10923.

[21] *** ASTM E8/E8M-16, *Standard Test Methods for Tension Testing of Metallic Materials*, ASTM International 2016, West Conshohocken, PA, USA.

[22] ***ANSI/AWS C1.1M/C1.1:2012, *Recommended Practices for Resistance Welding*, American Welding Society 2012, Miami, FL, USA.